G-FOLD: A Real-Time Implementable Fuel Optimal Large Divert Guidance Algorithm for Planetary Pinpoint Landing

Article · June 2012

CITATIONS
18

READS
16,276

4 authors:

Behçet Açıkmeşe
University of Washington Seattle
242 PUBLICATIONS **4,183** CITATIONS
SEE PROFILE

Jordi Casoliva
NASA
21 PUBLICATIONS **400** CITATIONS
SEE PROFILE

John M Carson
NASA
65 PUBLICATIONS **1,073** CITATIONS
SEE PROFILE

Lars Blackmore
SpaceX
51 PUBLICATIONS **2,531** CITATIONS
SEE PROFILE

AAS 13-386

FLIGHT TESTING OF TRAJECTORIES COMPUTED BY G-FOLD: FUEL OPTIMAL LARGE DIVERT GUIDANCE ALGORITHM FOR PLANETARY LANDING

Behçet Açıkmeşe[1], MiMi Aung[2], Jordi Casoliva[2], Swati Mohan[2], Andrew Johnson[2], Daniel Scharf[2], David Masten[3], Joel Scotkin[3], Aron Wolf[2], and Martin W. Regehr[2]

[1]Aerospace Engineering and Engineering Mechanics, The University of Texas at Austin, Austin, TX 78712, USA,

[2]Jet Propulsion Laboratory , California Institute of Technology, Pasadena, CA 91109, USA

[3]Masten Space Systems, Inc., Mojave, CA 93501, USA

G-FOLD, Guidance for Fuel Optimal Large Divert, is an algorithm that is developed to compute, onboard in real-time, fuel optimal trajectories for large divert maneuvers necessary for planetary pinpoint or precision landing. The algorithm incorporates all relevant mission constraints and computes the global optimal trajectory. It is based on a mathematical result known as "lossless convexification" of the associated optimal control problem, which allowed us to formulate the problem as a convex optimization problem and to guarantee obtaining the global optimal solution when a feasible solution exists. Hence the algorithm ensures that all physically achievable diverts are also computable in real-time. This paper reports the first three flight test results of G-FOLD generated trajectories. The goal of these tests were to test pre-flight computed G-FOLD trajectories to demonstrate that they are computed with relevant mission constraints and appropriate vehicle dynamics accounted for. The results showed good agreement with the desired ideal trajectories with mismatches below expected bounds, which validated that the desired outcome that the trajectories were computed by using the right problem description and the resulting trajectories are flyable.

INTRODUCTION

A fuel optimal guidance planetary powered descent algorithm is developed[1,2,3] to autonomously compute the fuel optimal path that takes the lander vehicle to a given surface target on a planet without violating any mission constraints. The algorithm is based on a fundamental result, known as lossless convexification,[2,4] that provides the solution of a general class of nonconvex optimal control problems, which includes planetary soft landing optimal control problem, via convex optimization methods. The resulting powered descent **G**uidance algorithm for **F**uel **O**ptimal **L**arge **D**iverts (**G-FOLD**) is needed for planetary pinpoint landing. It will enable access to unreachable but scientifically valuable targets for Mars sample return mission and to deliver large payloads necessary for human class planetary missions. Figure 1 summarizes the development history of the G-FOLD algorithm from conception to the flight testing. This paper describes the first flight testing of the trajectories generated by this algorithm and its results.

The main purpose of Guidance, Navigation, and Control (GN&C) during the landing phase of planetary missions is to reduce the lander's velocity from orbital or interplanetary velocities to

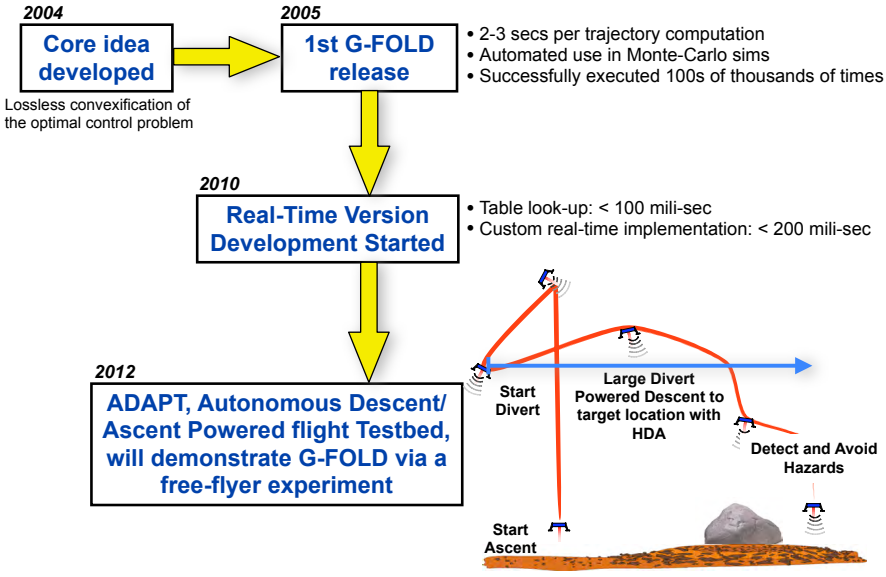

Figure 1. Development history of the G-FOLD algorithm

almost zero velocity. In case of planets with atmospheres (such as Mars), this first involves an entry phase (see Fig. 2), which cancels most of the surface relative velocity. Once the lander slows down to supersonic speeds, a parachute is deployed. Then at a prescribed altitude and velocity, the parachute is released and the Powered Descent phase is initiated. Due to atmospheric uncertainties in winds and density and due to the passive deceleration during the parachute phase, the position and velocity relative to the target is dispersed significantly and they cannot be predetermined. In the example of Mars landing, the distance error can be in the order of 8-10 km with the velocity trigger, used in Mars Science Laboratory (MSL), and 5-6 km with a range trigger for the start of parachute phase.[5,6] To achieve pinpoint landing (position error $<$ 100 m at touchdown), an autonomous guidance algorithm must be used to redirect the vehicle to the surface target in real-time to correct for these errors.

G-FOLD algorithm generates fuel optimal trajectories that correct the errors accumulated during planetary entry and descent. The trajectories generated will require large diverts to achieve pinpoint landing. This implies generating fuel optimal flight trajectories with large horizontal velocities and large tip angles for the lander to point the thrust vector in the desired direction. We tested such trajectories in an Earth based testbed, Autonomous Descent Ascent Powered flight Testbed (ADAPT)[7] in collaboration with Masten Space Systems, Inc., by using their vertical lander vehicle called "Xombie". There were three successful test flight performed. The vehicle ascended to about 480 meters altitude and then dropped to 450 meters, to attain desired descent velocity, and then diverted sideways by 550 meters,[8] 650 meters,[9] and 750[10] meters in three successive flights. The prior flights of Xombie have never diverted beyond 50 meters sideways. Additionally large horizontal velocities imply large aerodynamic torques on the vehicle, which cannot be handled with the current control authority beyond a certain velocity. Therefore we increased the maximum allowable horizontal velocity incrementally and kept the maximum magnitude of the velocity vector less than 26.8 meters/sec ($\approx$ 60 mph). In each flight we computed the maximum possible divert from 450 meter

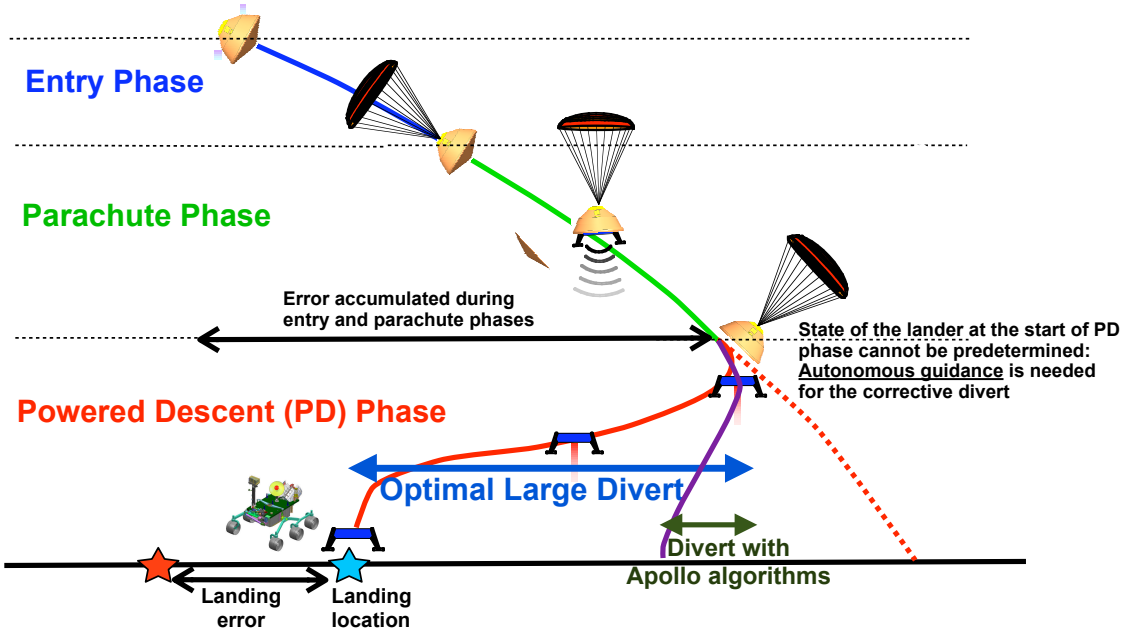

Figure 2. Optimal Powered Descent Guidance (PDG) will enable planetary pinpoint landing. It searches all physically possible diverts and significantly increases the divert capability over the current state-of-the-art onboard algorithms.

altitude and 16.8 meters/sec descent velocity to the ground, with successively increased horizontal velocity bounds of 16.8 meters/sec, 22.8 meters/sec, and 24.8 meters/sec. The flight data showed excellent agreement with the desired trajectories, which implied that the dynamics of the vehicle and the mission constraints are captured adequately in our trajectory optimization formulation and computations.

LARGE DIVERT GUIDANCE PROBLEM

The large divert guidance problem for soft landing is a finite horizon optimal control problem, where we search for the thrust vector profile $\mathbf{T}_c$ and an accompanying translational state trajectory $(\mathbf{r}, \dot{\mathbf{r}})$ that guide a lander from an initial position $\mathbf{r}_0$ and velocity $\dot{\mathbf{r}}_0$ to a state of rest at the prescribed target location on the planet while minimizing the fuel use. Here we consider a planet with a uniform gravity field, and we ignore aerodynamic forces during the powered-descent phase of landing. Clearly the ignoring of the aerodynamic forces on Earth is a source of inaccuracy. In our particular testing we bounded the velocity magnitude at a low value of $\approx$ 27 m/s, and we expected that ignoring the aerodynamic forces will not be detrimental due to this low maximum velocity bound.

In this problem there are several state and control constraints. The main state constraints are glide slope constraint on the position vector and an upper bound constraint on the velocity vector magnitude. The glide slope constraint is described in Figure 3 and it is imposed to ensure that the lander stays at a safe distance from the ground until it reaches its target. The upper bound on velocity is needed to avoid supersonic velocities for planets with atmosphere, where the control thrusters can become unreliable. Both of these constraints are convex and they fit well to the convex optimization framework considered in this paper. The control constraints, however, are challenging since they

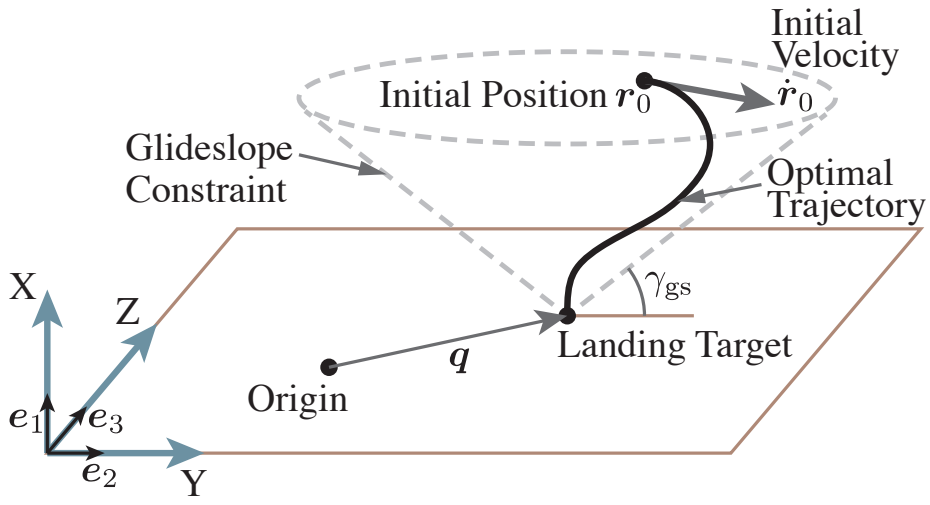

Figure 3. ***Glideslope constraint in minimum landing error powered descent guidance problem. The glide slope constraint requires the spacecraft to remain in a cone defined by the minimum slope angle γ. In the minimum landing error case, the apex of the cone coincides with the landed position of the spacecraft, rather than the original target.***

define a non-convex set of feasible controls. We have three control constraints (see Figure 4): Given any maneuver time (time-of-flight) t_f, for all $t \in [0, t_f]$

i) Convex upper bound on thrust, $\|\mathbf{T}_c(t)\| \leq \rho_2$.

ii) Non-convex lower bound on thrust, $\|\mathbf{T}_c(t)\| \geq \rho_1 > 0$.

iii) Thrust pointing constraint $\hat{\mathbf{n}}^T \mathbf{T}_c(t)/\|\mathbf{T}_c(t)\| \geq \cos\theta$ where $\|\hat{\mathbf{n}}\| = 1$ is a direction vector and $0 \leq \theta \leq \pi$ is the maximum allowable angle of deviation from the direction given by $\hat{\mathbf{n}}$, which is convex when $\theta \leq \pi/2$ and non-convex when $\theta > \pi/2$.

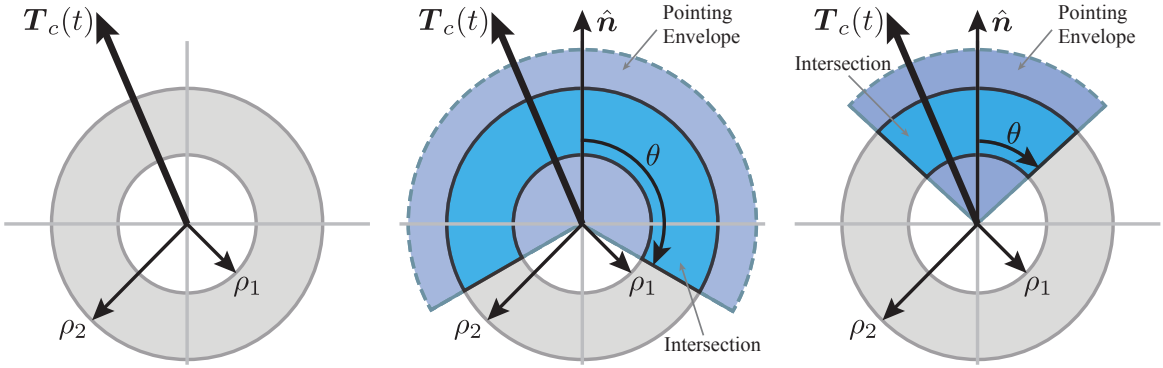

Figure 4. ***Planar representation of original thrust bounds (left) and intersection of thrust bounds and thrust pointing limits: $\theta \in (\pi/2, \pi]$ (middle) and $\theta \in [0, \pi/2]$ (right).***

Onboard sensors for terrain-relative navigation generally require specic viewing orientations, which imposes a constraint on the vehicle orientation (attitude). Since we model the vehicle as a point mass with a thrust vector, the required control force is applied by pointing the thrust vector along

the desired force direction. In this framework, we can impose constraints on the vehicle orientation by simply restricting the directions that the thrust vector can point to. This also avoids incorporating the attitude dynamics of the vehicle into the problem formulation, which would otherwise increase the problem complexity significantly. Considering attitude dynamics explicitly and imposing the pointing constraints directly, rather than on the thrust direction, can be a part of future research, which can benefit from the recent convexification results on the constrained attitude control.[11]

As mentioned earlier, the lander is modeled as a lumped mass with a thrust vector for control, and its dynamics are described by

$$\begin{aligned} \dot{\mathbf{x}}(t) &= A\,\mathbf{x}(t) + B\left(\mathbf{g} + \frac{\mathbf{T}_c(t)}{m(t)}\right) \\ \dot{m}(t) &= -\alpha\|\mathbf{T}_c(t)\| \end{aligned} \tag{1}$$

where $\mathbf{x}(t) = (\mathbf{r}(t),\, \dot{\mathbf{r}}(t)) : \mathbb{R}_+ \to \mathbb{R}^6$, $m(t) : \mathbb{R}_+ \to \mathbb{R}_+$ is the mass of the lander,

$$A = \begin{bmatrix} \mathbf{0} & \mathbf{I} \\ \mathbf{0} & \mathbf{0} \end{bmatrix}, \quad B = \begin{bmatrix} \mathbf{0} \\ \mathbf{I} \end{bmatrix}, \tag{2}$$

$\mathbf{g} \in \mathbb{R}^3$ is the constant gravity vector, and $\alpha > 0$ is a constant that describes the fuel consumption (mass depletion) rate. Here the time derivatives of the vectorial quantities are expressed in a planet surface fixed frame that has the planet's angular rotation rate and we also used the rocket equation which relates the fuel mass consumption rate to the applied thrust vector.[12]

We use a point mass model of the landing vehicle, where the translational dynamics are decoupled from rotational (attitude) dynamics. This is a common assumption used in practice mainly because the attitude control authority is typically far more high bandwidth than that of the translational control. Specifically any attitude maneuver required to point the thruster in the right direction for translational control can be performed very quickly such that the interaction between the attitude and translational control systems are minimal. As a result, this is a reasonable assumption that reduces the problem complexity.

Given the constraints and the dynamics the planetary soft landing problem can be formulated as follows:

Problem 1 Non-Convex Minimum Fuel Planetary Landing Problem

$$\max_{t_f, \mathbf{T}_c} \; m(t_f) \qquad \text{subject to:} \tag{3}$$

$$\left.\begin{aligned} \dot{\mathbf{x}}(t) = A\mathbf{x}(t) + B\left(\mathbf{g} + \frac{\mathbf{T}_c(t)}{m}\right) \\ \dot{m}(t) = -\alpha\|\mathbf{T}_c(t)\| \end{aligned}\right\} \quad \forall\, t \in [0, t_f], \tag{4}$$

$$\mathbf{x}(t) \in \mathbf{X} \qquad \forall\, t \in [0, t_f], \tag{5}$$

$$0 < \rho_1 \le \|\mathbf{T}_c(t)\| \le \rho_2, \quad \hat{\mathbf{n}}^T \mathbf{T}_c(t) \ge \|\mathbf{T}_c(t)\| \cos\theta, \tag{6}$$

$$m(0) = m_0 \tag{7}$$

$$\mathbf{r}(0) = \mathbf{r}_0, \quad \dot{\mathbf{r}}(0) = \dot{\mathbf{r}}_0, \tag{8}$$

$$\mathbf{r}(t_f) = 0, \quad \dot{\mathbf{r}}(t_f) = \mathbf{0}. \tag{9}$$

In the above problem $\mathbf{X}$ defines the state constraints and it is given by

$$\mathbf{X} = \left\{ (\mathbf{r}, \dot{\mathbf{r}}) \in \mathbb{R}^6 : \tan\gamma \mathbf{e}_1^T \mathbf{r} \geq \sqrt{(\mathbf{e}_2^T \mathbf{r})^2 + (\mathbf{e}_3^T \mathbf{r})^2},\ \|\dot{\mathbf{r}}\| \leq V_{max},\ |\mathbf{e}_i^T \dot{\mathbf{r}}| \leq V_h,\ i = 2, 3 \right\},$$

V_{max} is maximum allowed velocity, V_h is the maximum allowable horizontal velocity, $\mathbf{e}_1$ is the unit vector along the x-axis (vertical axis), $\mathbf{e}_2$ and $\mathbf{e}_3$ are unit vectors in y and z directions. Note that the control constraints are non-convex in Problem 1 as also depicted in Figure 4.

SUMMARY OF THE SOLUTION METHOD USED IN G-FOLD

In this section we will present the highlights of the "lossless convexification" method to convert the optimal control problem into an equivalent problem with convex control constraints. This is achieved by using a particular convex relaxation of the control constraints.[1,2,4,3]

Problem 2 Convex Relaxed Minimum Fuel Landing Problem

$$\max_{t_f, \mathbf{T}_c, \Gamma} m(t_f) \qquad \text{subject to (5), (7), (8), (9), and}$$

$$\left.\begin{aligned} \dot{\mathbf{x}}(t) &= A\mathbf{x}(t) + B\left(\mathbf{g} + \frac{\mathbf{T}_c(t)}{m}\right) \\ \dot{m}(t) &= -\alpha\Gamma(t) \end{aligned}\right\} \quad \forall\, t \in [0, t_f], \tag{10}$$

$$\|\mathbf{T}_c(t)\| \leq \Gamma(t),\ 0 < \rho_1 \leq \Gamma(t) \leq \rho_2, \tag{11}$$

$$\hat{\mathbf{n}}^T \mathbf{T}_c(t) \geq \cos\theta\, \Gamma(t), \tag{12}$$

In the relaxed problem we introduced a slack variable to lifting the control space to a higher dimension (with one additional dimension) and relaxing the non-convex set of controls to a convex set. Figure 5 describes the geometric insight behind the convexification. In summary the Hamiltonian must be maximized at every time instant according to the Pontryagin's Maximum Principle.[13] This boils down to maximizing $y^T \mathbf{T}_c$ where y is a part of the costate defined as a part of the Maximum Principle. And in our earlier work [14], we proved that this will lead to having the optimal controls on the extremal points of the relaxed convex set, and it turns out that the extreme points are in the original non-convex set of controls. Since the relaxed control set includes the original one, and all the optimal solutions of Problem 2 satisfy the constraints of Problem 1, the optimal solutions of the relaxed problem are also optimal for the original one. This leads to the desired conclusion of the lossless convexification (see [2, 4, 3, 14] for the mathematical details).

Once we establish the lossless convexifictaion result, next step is to discretize the optimal control problem in a form that is amenable to using Interior Point Methods (IPM) of convex optimization. The details of the problem discretization to convert the infinite dimensional optimal control problem to a finite dimensional convex optimization problem can be found in [2, 3]. IPMs are powerful computational methods that establish guarantees of obtaining global optimal solutions of convex optimization problems to any accuracy in polynomial time,[15,16,17] that is, as the problem size increases the computational complexity increases gracefully. And recent advances in real-time convex optimization[18] proved that custom algorithms can solve small to medium size of convex optimization problems in the order of micro to milliseconds, which make them, with the guarantees of convergence, ideal for real-time onboard use.

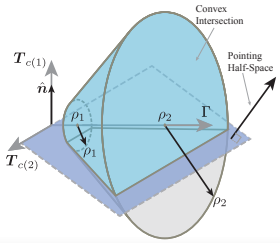

Hamiltonian is maximized at the **extreme points** of the relaxed set ensuring that the original constraints are satisfied

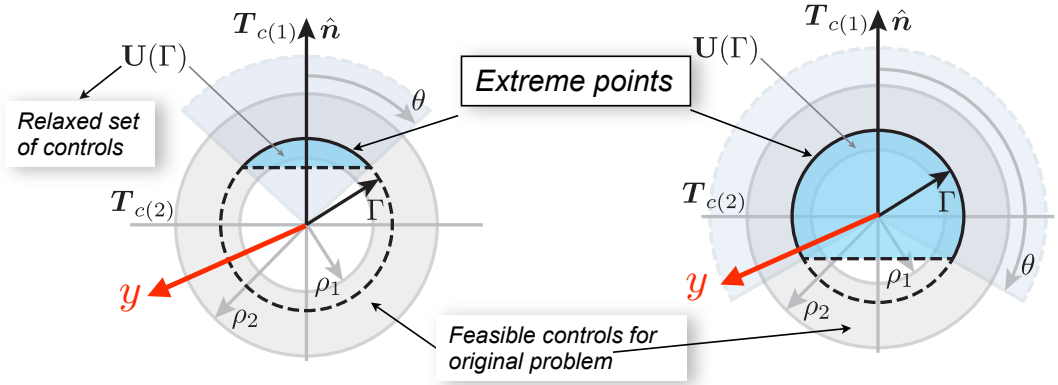

Figure 5. Relaxation of the non-convex control set to a convex set. Planar representation of $\mathbf{U}(\Gamma) = \{\mathbf{T}_c : \|\mathbf{T}_c\| \leq \Gamma,\ \hat{\mathbf{n}}^T\mathbf{T}_c(t) \geq \cos\theta\,\Gamma\}$: $\theta \in (\pi/2, \pi]$ (left) and $\theta \in [0, \pi/2]$ (right). Extreme points of $\mathbf{U}(\Gamma)$ satisfy that $\|\mathbf{T}_c\| = \Gamma$, and they are on the solid arc in both cases. The optimal solutions of Problem 2 are proven to be on these extreme points, hence they are feasible for Problem 1. Since the set of feasible controls is embedded in the set of feasible controls of Problem 2, this implies that the optimal solutions of the relaxed problem define optimal solution of the original minimum fuel problem. Therefore the convexification is lossless and we can utilize IPM algorithms to solve for the global optimal solutions of Problem 1 onboard in real-time.

TEST RESULTS

This section describes the experimental results. As mentioned earlier, we had three flight experiments:

- Test-1: 500 meter divert,[8] see Figure 7
- Test-2: 650 meter divert,[9] see Figure 8
- Test-3: 750 meter divert,[10] see Figure 9

The fuel optimal trajectories are generated offline and loaded on the flight computer. Then the onboard feedback control algorithms for attitude and translation ensured that the optimal trajectories are followed to a desirable accuracy. The tracking performance data is given in Tables 2 and 1. The maximum position error along any axis was less than 1 meter over a 750 meters of divert, which was very satisfactory. The vehicle was flown as far as possible by ensuring that 15 kg of spare fuel would be left nominally, by obeying the following control and velocity constraints:

- Test-1: $V_{max} = 26.7$, $V_h = 16.7$, $\theta = 30$
- Test-2: $V_{max} = 26.7$, $V_h = 22.7$, $\theta = 30$
- Test-3: $V_{max} = 26.7$, $V_h = 24.7$, $\theta = 30$

Flight	$\delta\mathbf{r}_1$	$\delta\mathbf{r}_2$	$\delta\mathbf{r}_3$	$\delta\dot{\mathbf{r}}_1$	$\delta\dot{\mathbf{r}}_2$	$\delta\dot{\mathbf{r}}_3$
500 m	0.1833	0.1386	0.2147	0.1750	0.0268	0.1286
650 m	0.2413	0.1273	0. 5402	0.1500	0.1121	0.2703
750 m	0.3987	0.1281	0.5168	0.3421	0.0410	0.3187

Table 1. Standard Deviation of the position and velocity errors per axis

Flight	$\max\lvert\delta\mathbf{r}_1\rvert$	$\max\lvert\delta\mathbf{r}_2\rvert$	$\max\lvert\delta\mathbf{r}_3\rvert$	$\max\lvert\delta\dot{\mathbf{r}}_1\rvert$	$\lvert\max\delta\dot{\mathbf{r}}_2\rvert$	$\lvert\max\delta\dot{\mathbf{r}}_3\rvert$
500 m	0.6783	0.5824	0.4495	0.4284	0.1440	0.3142
650 m	0.7716	0.2458	1.3362	0.7689	0.2708	0.5822
750 m	0.7425	0.3399	0.9827	1.0538	0.1208	1.2407

Table 2. Maximum position and velocity errors per axis

The overall control system has the following hierarchical structure (see Figure 6): The optimal trajectories provided the nominal desired position and velocity profiles, $p_d : [0, t_f] \to \mathbb{R}^3$ and $v_d[0, t_f] \to \mathbb{R}^3$, to be followed by the vehicle. It also provided a nominal force vector that must be applied, $F_o : [0, t_f] \to \mathbb{R}^3$. In real-time, the estimates of the position and velocity vectors, $\hat{p}$ and $\hat{v}$, are obtained by the state state estimator using real-time GPS and IMU data. Then a feedback force factor is computed by a translational feedback controller:

$$F_f(t) = \mathcal{F}(\hat{p}(t) - p_d(t), \hat{v}(t) - v_d(t)), \quad t \in [0, t_f]$$

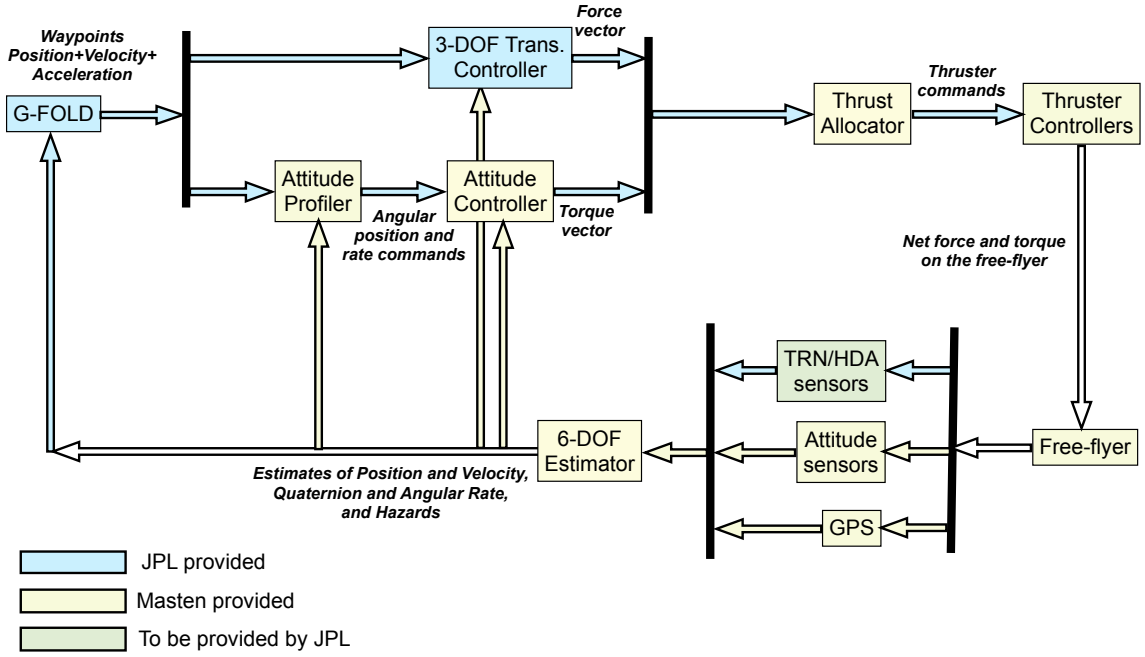

Figure 6. Guidance, Navigation, and Control block diagram shows the interplay between different algorithmic components on the flight software of the vehicle (free-flyer). Here TRN/HDA refers to the Terrain Relative Sensor and Hazard Detection and Avoidance to be provided by JPL in the future flights. 3-DOF and 6-DOF denote three and six Degrees-Of-Freedoms. Thrust allocator computes the thruster commands, the gimbal mangle and the thrust (throttle) level.

where $\mathcal{F}$ represents a dynamic filter, which is a combination of a PID controller with a low-pass filter and t_f is the total flight time. Then the overall translational control force that must be applied is computed as follows:

$$F = F_o + F_f.$$

However we have a single gimbaled thruster with about 7 degrees of gimbaling capability along two independent axes. The way that the force vector F is used is as follows: The force magnitude goes to the thruster as a throttle command so that the thruster provides the right force magnitude. The direction of the force goes to the attitude controller as a direction command, which is then converted to a feedback torque command. The feedback torque command is then converted into a gimbal angle command for the thruster. Consequently this process produces both the throttle and gimbals commands needed by the thruster. Therefore the force vector F has always some inherent delay based on the bandwidth of the attitude controller. The tracking results demonstrated that the particular controllers used provided very good performance as seen in Figures 7, 8, and 9 and Tables 2 and 1.

An interesting observation is made in the comparisons of the actual versus the nominal force magnitudes, which are presented in Figures 7, 8, and 9. There is almost a constant offset between these values in all three flight in two distinct time intervals that correspond to constant velocity portions of the flights. Note that we computed the optimal trajectories by ignoring the aerodynamic drag forces, due to limited velocities (< 26.7 m/s). In the first constant velocity portion of all flights (approximately $t \in (10, 30)$ secs), the velocity is about 15.7 m/s and in the second constant

velocity regime the velocities are 16.7 m/s in Test-1, 22.7 m/s in Test-2, and 24.7 m/s in Test-3. This is indeed an expected offset due to ignoring the drag force which will be approximately constant during these two portions of the flight where the velocities are approximately constant. Hence what is ignored in optimal trajectory computations, which is drag force, manifested itself as expected. Furthermore it is also noteworthy to observe that, in the first portion, the actual force is more than desired, since the vehicle is fighting against drag during its initial ascent. In the second portion, the actual force is less than the desired. The reason for that is the tail winds that we experienced in all of these flights due to the position launch and landing pads and the expected velocity fields in the particular test location. We indeed measured tail winds during these experiments.

In summary the tests were conducted successfully and the results were in excellent agreement with our predictions. These tests motivated the next step of putting the real-time convex optimization based guidance algorithm G-FOLD onboard and executing it in real-time, which will be the focus of next set of flight tests in 2013.

CONCLUSIONS

This paper presented the first test flight results for G-FOLD, Guidance for Fuel Optimal Large Divert, algorithm. Three flights were performed with precomputed, by G-FOLD, large divert trajectories. The predicted and actual trajectories were shown to be in excellent agreement. This proved that we captured the dynamics and the constraints of the actual flight well. More importantly, G-FOLD prove to be enabling by computing trajectories with an order of magnitude larger diverts than previously flown by this test vehicle. Hence it utilized the capabilities of the vehicle to the fullest extent without violating any of the mission or vehicle constraints.

Our next step in this testing is to generate optimal trajectories onboard in realtime by using the flight version of the G-FOLD solution algorithm customized for ADAPT tests. This will prove that a convex optimization based guidance algorithm that incorporates a realistic dynamical model of the vehicle as well as all the relevant mission constraints can be executed autonomously onboard in realtime. The maturation of this onboard guidance capability for flight use will provide a key enabling technology for many exciting planetary landing missions.

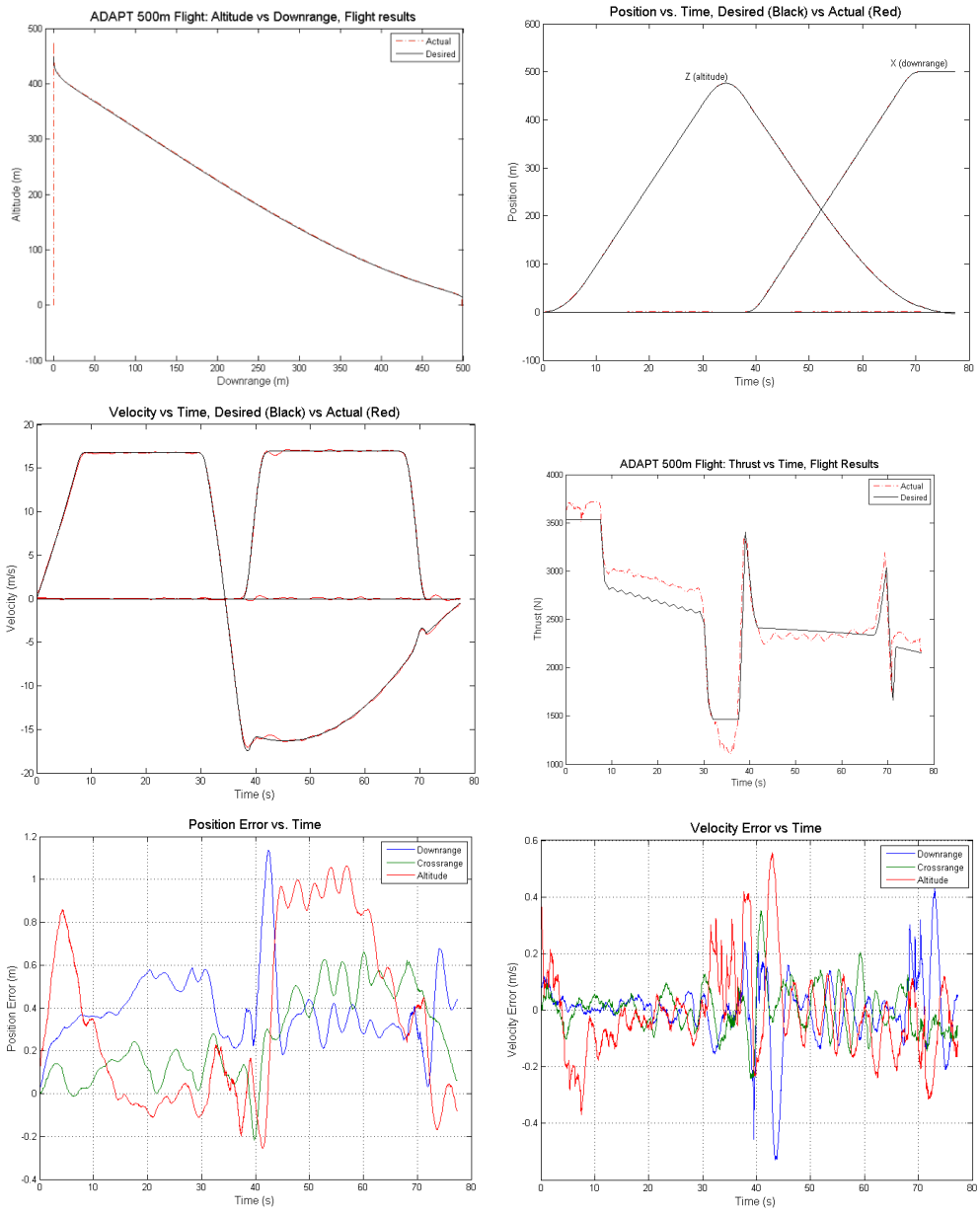

Figure 7. Test-1: The results for 500 meter divert flight test. "Black" lines represent the desired trajectory quantities and "red "lines represent the actual test results. Top left plot presents altitude versus downrange trajectory, top right plot presents the position components as a function of time, middle left plot presents the position components as a function of time, the middle right presents the force vector components as a function of time, and the bottom row plots are for position and velocity errors relative to the desired trajectory.

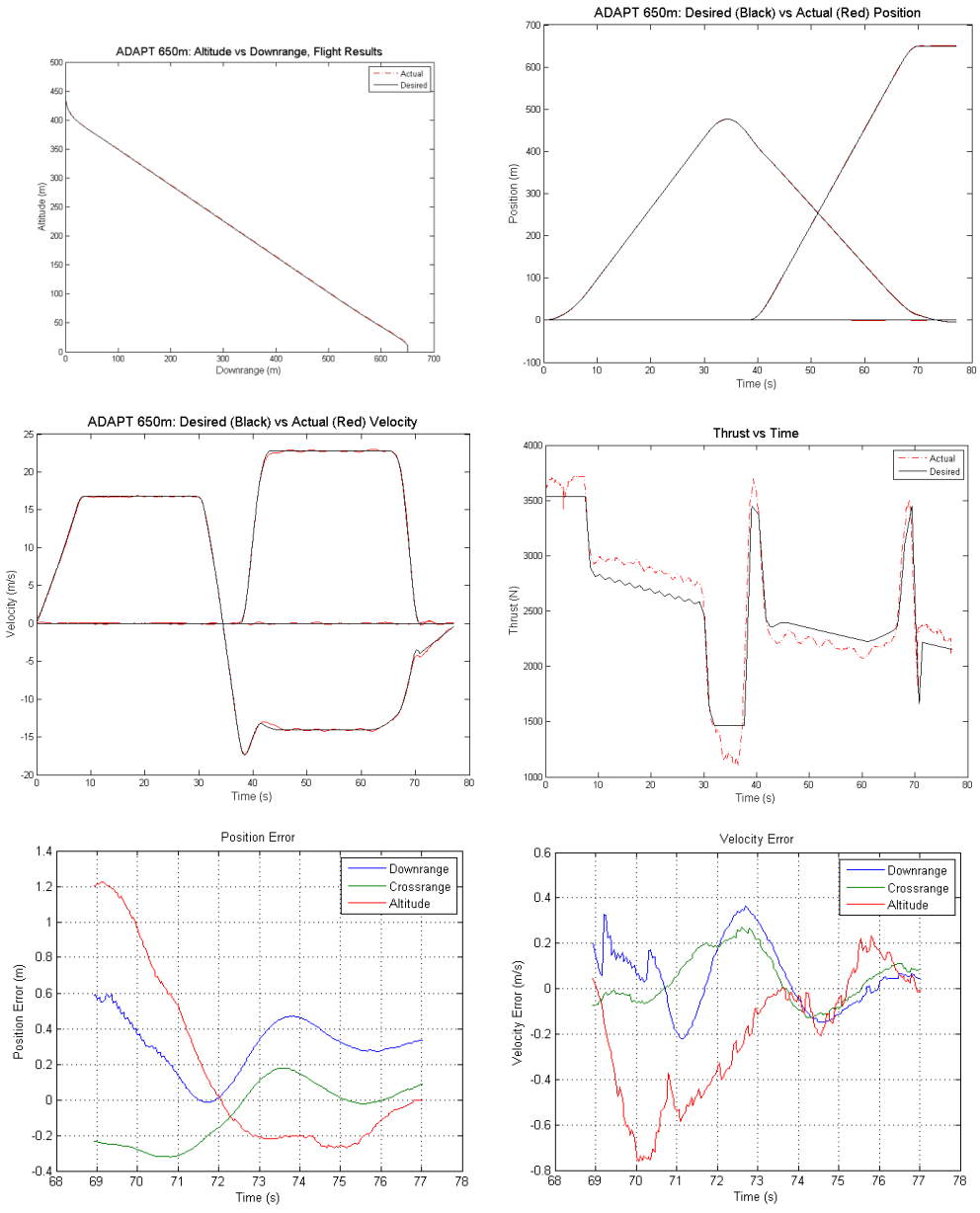

Figure 8. Test-2: The results for 650 meter divert flight test. "Black" lines represent the desired trajectory quantities and "red "lines represent the actual test results. Top left plot presents altitude versus downrange trajectory, top right plot presents the position components as a function of time, middle left plot presents the position components as a function of time, the middle right presents the force vector components as a function of time, and the bottom row plots are for position and velocity errors relative to the desired trajectory.

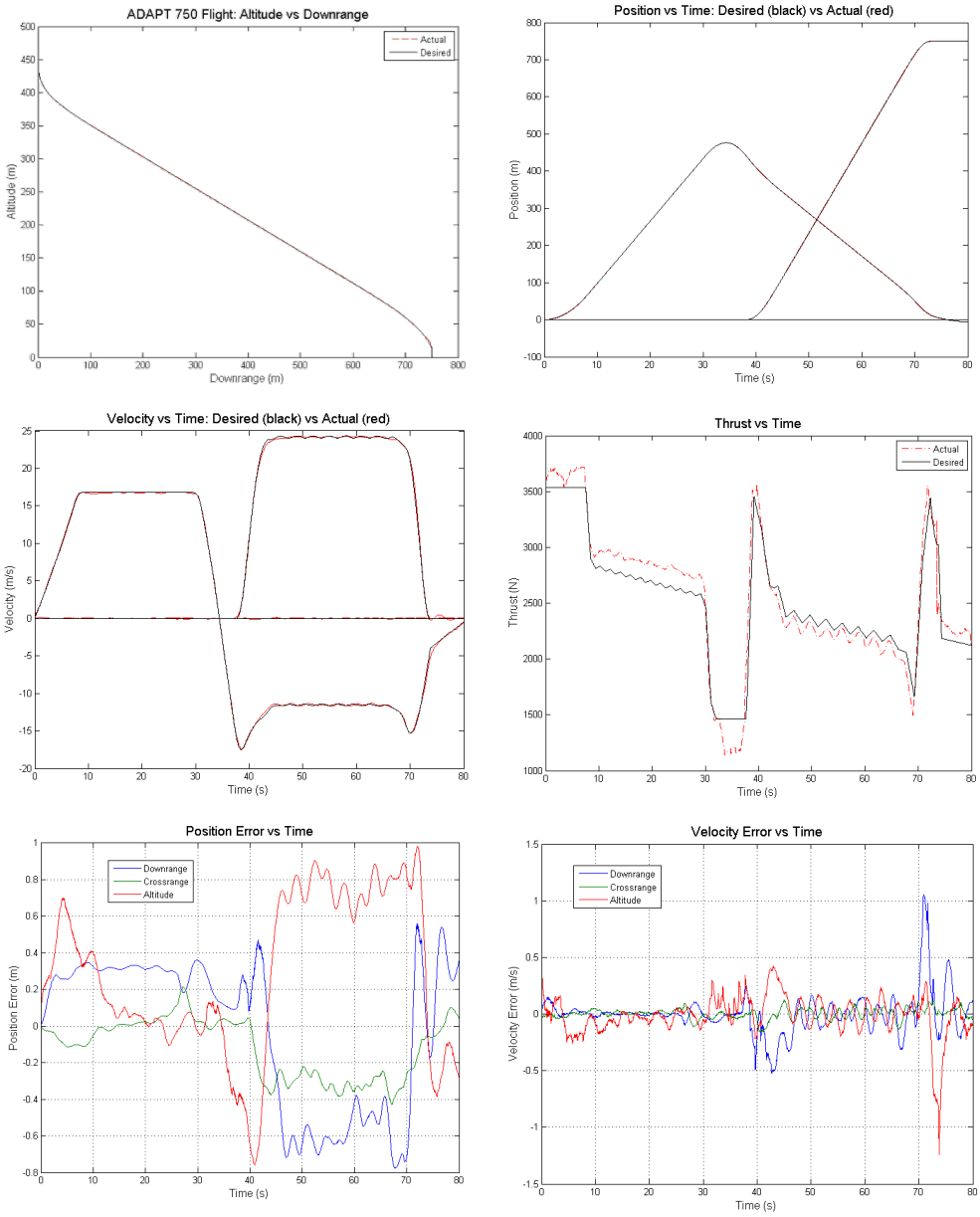

Figure 9. Test-3: The results for 750 meter divert flight test. "Black" lines represent the desired trajectory quantities and "red "lines represent the actual test results. Top left plot presents altitude versus downrange trajectory, top right plot presents the position components as a function of time, middle left plot presents the position components as a function of time, the middle right presents the force vector components as a function of time, and the bottom row plots are for position and velocity errors relative to the desired trajectory. The agreement between the desired and actual measured trajectories is excellent, as in the 500 and 650 meter flights. In all of the experiments, the control forces applied versus desired have a constant offset at different flight velocity regimes, indicating that the feedback controllers were canceling aerodynamic force effects that were not accounted in the trajectory optimization. The aerodynamic forces are treated as disturbances because of the bounds imposed the sideways velocities.

REFERENCES

[1] B. Açıkmeşe and S. R. Ploen, "A powered descent guidance algorithm for Mars pinpoint landing," *AIAA Guidance, Navigation, and Control Conference and Exhibit, San Francisco*, 2005.

[2] B. Açıkmeşe and S. R. Ploen, "Convex Programming Approach to Powered Descent Guidance for Mars Landing," *AIAA Journal of Guidance, Control and Dynamics*, Vol. 30, No. 5, 2007, pp. 1353–1366.

[3] L. Blackmore, B. Açıkmeşe, and D. P. Scharf, "Minimum Landing Error Powered Descent Guidance for Mars Landing using Convex Optimization," *AIAA Journal of Guidance, Control and Dynamics*, Vol. 33, No. 4, 2010.

[4] B. Açıkmeşe and L. Blackmore, "Lossless convexification for a class of optimal control problems with nonconvex control constraints," *Automatica*, Vol. 47, No. 2, 2011, pp. 341–347.

[5] D. Way, "On the use of a range trigger for the Mars Science Laboratory entry, descent, and landing," *2011 IEEE Aerospace Conference, Paper 1142*, 2011.

[6] B. A. Steinfeld, M. J. Grant, D. A. Matz, R. D. Braun, and G. H. Barton, "Guidance, navigation, and control system performance trades for Mars pinpoint landing," *AIAA Journal of Spacecraft and Rockets*, Vol. 47, No. 1, 2010, pp. 188–198.

[7] M. Aung, B. Açıkmeşe, A. E. Johnson, M. W. Regehr, J. Casoliva, S. Mohan, A. Wolf, D. Masten, and J. Scotkin, "A closed-loop testbed for next-generation EDL GNC systems," *AAS/AIAA Space Flight Mechanics Conference, Hawaii*, February 2013.

[8] M. S. Systems and N. J. P. Laboratory, "500 meter test flight video of Xombie," *http://www.youtube.com/watch?v=1GRwimo1AwY*, July 2012.

[9] M. S. Systems and N. J. P. Laboratory, "650 meter test flight video of Xombie," *http://www.youtube.com/watch?v=WU4TZlA3jsg*, August 2012.

[10] M. S. Systems and N. J. P. Laboratory, "750 meter test flight video of Xombie," *http://www.youtube.com/watch?v=jl6pw2oossU*, August 2012.

[11] Y. Kim and M. Mesbahi, "Quadratically Constrained Attitude Control via Semidefinite Programming," *IEEE Transactions on Automatic Control*, Vol. 49, No. 5, 2004, pp. 731–735.

[12] G. P. Sutton and O. Biblarz, *Rocket Propulsion Elements*. Wiley, 2010.

[13] L. D. Berkovitz, *Optimal Control Theory*. Springer-Verlag, 1975.

[14] J. M. Carson, B. Açıkmeşe, and L. Blackmore, "Lossless Convexification of Powered-Descent Guidance with Non-Convex Thrust Bound and Pointing Constraints," *In Proceedings of American Control Conference*, 2011.

[15] S. Boyd and L. Vandenberghe, *Convex Optimization*. Cambridge University Press, 2004.

[16] Y. Nesterov and A. Nemirovsky, *Interior-point Polynomial Methods in Convex Programming*. SIAM, 1994.

[17] J. Peng, C. Roos, and T. Terlaky, *Self-Regularity: A New Paradigm for Primal-Dual Interior-Point Algorithms*. Princeton Series in Applied Mathematics, 2001.

[18] J. Mattingley and S. Boyd, "Real-time Convex Optimization in Signal Processing," *IEEE Signal Processing Magazine*, Vol. 27, No. 3, 2010, pp. 50–61.